JOURNAL OF SPACECRAFT AND ROCKETS
Vol. 41, No. 5, September–October 2004

Six-Degree-of-Freedom Modeling of Semi-Autonomous Attitude Control During Aerobraking

Wyatt R. Johnson* and James M. Longuski†
Purdue University, West Lafayette, Indiana 47907-1282
and
Daniel T. Lyons‡
Jet Propulsion Laboratory, California Institute of Technology, Pasadena, California 91109-8099

The automation of a Mars aerobraking vehicle that uses reaction wheels for attitude and angular momentum control during atmospheric flythrough is investigated. In a previous study, single-axis control laws were developed for minimum onboard instrumentation to compensate for large variations in entry time and atmospheric density. Modifications of those control laws to provide two-axis control in high-fidelity simulations that include six degrees of freedom, nearly ideal reaction wheels, spherical harmonics, and oblate atmosphere are now tested. Preliminary results indicate that our approach may be highly practical for an autonomous aerobraking mission at Mars.

Nomenclature

A	=	reaction wheel orientation matrix, or system matrix
B	=	input matrix
C	=	fully normalized tesseral coefficient, or output matrix
C_D	=	coefficient of drag
C_{M_x}	=	partial of moment coefficient with respect to sideslip angle, deg^{-1}
C_{M_y}	=	partial of moment coefficient with respect to angle of attack, deg^{-1}
D	=	direction cosine matrix
$\boldsymbol{E}$	=	relative Euler angles, rad
e	=	eccentricity
$\boldsymbol{F}$	=	affine term in equations of motion, rad/s
f	=	reaction wheel friction torque coefficient
$\boldsymbol{H}$	=	total angular momentum, kg · m^2/s
I	=	spacecraft (with reaction wheels) inertia matrix, kg · m^2
$\tilde{I}$	=	spacecraft (without reaction wheels) inertial matrix, kg · m^2
J	=	diagonal matrix of reaction wheel moments of inertia, kg · m^2
K	=	feedback gain matrix
L	=	reference length, m
$\boldsymbol{M}$	=	external moment acting on spacecraft, N · m
P	=	fully normalized associated Legendre function
q	=	dynamic pressure, N/m^2
$\boldsymbol{q}$	=	inertial attitude quaternion
$\boldsymbol{r}$	=	inertial position vector of spacecraft, km
S	=	fully normalized sectoral coefficient, or reference area, m^2
U	=	gravity potential, km^2/s^2
$\boldsymbol{u}$	=	reaction wheel control torques, N · m
$\boldsymbol{V}$	=	inertial velocity vector of spacecraft, km/s
$\boldsymbol{x}$	=	state vector
α	=	angle of attack, deg
β	=	sideslip angle, deg
γ	=	flight path angle, deg
$\Delta\boldsymbol{V}$	=	change in velocity vector, m/s
θ	=	true anomaly plus argument of periapsis, deg
λ	=	International Astronomical Union (IAU) longitude, °
μ	=	gravitational parameter, km^3/s^2
ρ	=	atmospheric density, kg/km^3
ϕ	=	IAU latitude, °
χ	=	$\theta - \gamma$, deg
ψ	=	roll angle, deg
$\boldsymbol{\Omega}$	=	reaction wheel angular rates, deg/s
$\boldsymbol{\omega}$	=	spacecraft angular rates, deg/s

Subscripts

atm	=	atmospheric
p	=	periapsis
Q	=	quaternion kinematical matrix
rel	=	relative motion

Superscripts

cm	=	center of mass
e	=	equilibrium
i	=	inertial
$\times$	=	cross product matrix

Received 12 November 2002; revision received 22 June 2003; accepted for publication 21 July 2003.

*Ph.D. Candidate, School of Aeronautics and Astronautics; currently Senior Engineer, Navigation and Mission Design, Jet Propulsion Laboratory, California Institute of Technology, 4800 Oak Grove Drive, Pasadena, CA 91109-8099. Member AIAA.

†Professor, School of Aeronautics and Astronautics. Associate Fellow AIAA.

‡Senior Engineer, Navigation and Mission Design, 4800 Oak Grove Drive.

Introduction

AEROBRAKING saved the Mars Global Surveyor (MGS) (Fig. 1) 1200 m/s of propulsive ΔV (about 380 kg of propellant) in placing a spacecraft into a low-energy orbit around Mars.[1–5] Similar aeroassisted techniques in the literature also provide reduction in propulsive maneuvers.[6–8]

An aerobraking spacecraft uses the atmosphere to reduce the energy of the orbit (Fig. 2). The atmospheric drag force provides the desirable ΔV to effect the orbit change. During each orbit, the spacecraft also accumulates angular momentum from several external torques, for example, aerodynamic, gravity gradient, and solar radiation pressure. Traditionally, the spacecraft reaction wheels absorb this angular momentum, allowing the spacecraft itself to remain in an inertial attitude. As the reaction wheels become saturated, propellant is used to eliminate the acquired angular momentum.[9]

In our scenario, we use the atmospheric torque to our advantage.[10,11] Instead of acquiring additional momentum during the drag pass, the spacecraft obtains a free desaturation of the reaction wheels by torquing against the atmosphere. Our goal is to

Table 1 Reference spacecraft parameters

Parameter	Reference value
Mass	1000 kg
C_D	1.9
C_{M_x}	$-0.01\ \text{deg}^{-1}$
C_{M_y}	$-0.00366\ \text{deg}^{-1}$
S	$17.44\ \text{m}^2$
L	8.73 m
Maximum RW torque	$0.18\ \text{N} \cdot \text{m}$
RW capacity	$27.0\ \text{N} \cdot \text{m} \cdot \text{s}$
I_{xx}	$814\ \text{kg} \cdot \text{m}^2$
I_{yy}	$410\ \text{kg} \cdot \text{m}^2$
I_{zz}	$695\ \text{kg} \cdot \text{m}^2$
J	$0.0645\ \text{kg} \cdot \text{m}^2$
f	$1 \cdot 10^{-6}\ \text{N} \cdot \text{m} \cdot \text{s}$

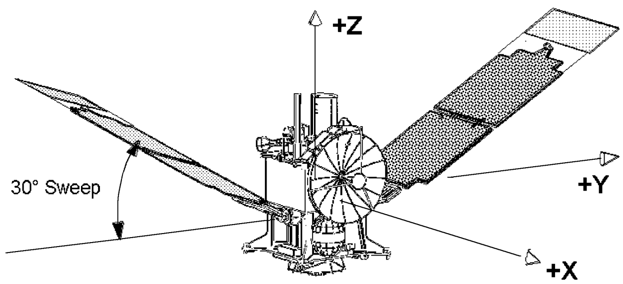

Fig. 1 MGS spacecraft.

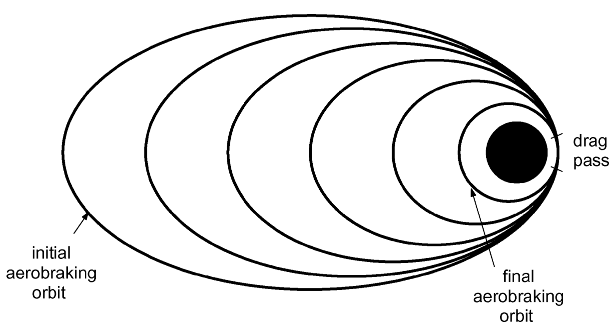

Fig. 2 Orbit decay using aerobraking.

devise a control law for the reaction wheels such that the net spacecraft momentum after each flythrough is driven to zero. Ideally, the spacecraft would have sufficient instrumentation available to measure every state variable. Unfortunately, such instrumentation comes at the expense of additional hardware cost and mass to the mission. We, therefore, choose to find a controller that will only rely on angular rate feedback.

Modeling Assumptions

Throughout the paper, we make the following modeling assumptions: 1) The only measurable states are spacecraft and reaction wheel angular rates and the inertial quaternion vector. 2) The Martian gravity field is evaluated up to 10th order and degree from a spherical harmonic model. 3) The spacecraft has three reaction wheels, which span $\mathcal{R}^3$. 4) The reaction wheels are aligned in arbitrary (possibly nonorthogonal) orientation, subject to the $\mathcal{R}^3$ constraint. 5) The reaction wheels are nearly ideal.[12] (No nonlinearities are present in reaction-wheel modeling.) 6) The reaction wheels are located at the spacecraft center of mass. 7) The atmosphere rotates as a rigid body along with Mars. 8) The atmosphere is modeled as oblate and locally exponential (using MarsGRAM COSPAR data[13,14]). 9) The controller provides control about the two aerodynamically stable axes only (pitch and yaw), that is, no attempt is made to control rotation about the roll axis. 10) The reference spacecraft properties are given in Table 1. 11) The equations of motion are integrated using an adaptive stepsize Runge–Kutta 4,5 method with a relative tolerance of 10^{-12}.

Equations of Motion

Orbital

The inertial position of the spacecraft is described in Cartesian coordinates by the International Astronomical Union convention.[15] The inertial X–Y plane is fixed in the equatorial plane of Mars, with the X direction defined by the intersection of the ecliptic and the equator. The Z direction is along the Martian north pole.

The three position equations of motion (EOMs) are simply

$$\dot{\boldsymbol{r}} = \boldsymbol{V} \tag{1}$$

The three velocity EOMs may be written as

$$\dot{\boldsymbol{V}} = -\nabla U + (\rho S C_D / 2m)\|\boldsymbol{\omega}_{\text{atm}} \times \boldsymbol{r} - \boldsymbol{V}\|(\boldsymbol{\omega}_{\text{atm}} \times \boldsymbol{r} - \boldsymbol{V}) \tag{2}$$

where $\boldsymbol{\omega}_{\text{atm}}$ is the rotation rate of Mars and U is the gravity potential given by

$$U = -\frac{\mu}{r}\left\{1 + \sum_{n=1}^{\infty}\sum_{m=0}^{n}\left(\frac{R}{r}\right)^n P_{nm}(\sin\phi)\cdot[C_{nm}\cos m\lambda + S_{nm}\sin m\lambda]\right\} \tag{3}$$

During each aeropass, the atmospheric drag forces dominate over the gravity perturbations. However, Olympus Mons (a 24-km-high volcano) can cause detectable changes to a spacecraft's orbit. For this reason, we evaluate the gravity potential up to 10th order and degree, which is needed to resolve Olympus Mons.

Attitude

We can express the spacecraft's attitude either inertially (using quaternions), or in terms of relative wind angles (such as angle of attack and sideslip angle). The spacecraft itself will not be able to measure these relative wind angles, but they are important from an analytical point of view, because the momentum EOMs are coupled with the relative wind angle EOMs.

Both sets of attitude EOMs require angular rate information, which is obtained from the momentum EOM. The total system angular momentum consists of two components: one due to the angular rate of the spacecraft relative to the inertial frame and the other due to the reaction wheels rotating relative to the spacecraft frame. The total momentum is, thus,

$$^{i}\boldsymbol{H}^{\text{cm}} = I\boldsymbol{\omega} + AJ\boldsymbol{\Omega} \tag{4}$$

Because the reaction wheels can only spin about one principal axis, only a single moment of inertia is needed to describe a reaction wheel. The J matrix is a 3×3 diagonal matrix of reaction wheel moments of inertia. The reaction wheel orientation matrix A maps unit vectors from the individual reaction wheel spin axes to the body-fixed frame. Because the reaction wheel spin axis directions are linearly independent, A is invertible.

To continue developing the attitude EOMs, we apply Euler's law to the entire system and then to the reaction wheels. For the spacecraft system, the momentum vector in Eq. (4) is differentiated with respect to the inertial frame to yield

$$^{i}\dot{\boldsymbol{H}}^{\text{cm}} = \boldsymbol{M}^{\text{cm}} = I\dot{\boldsymbol{\omega}} + AJ\dot{\boldsymbol{\Omega}} + \omega^{\times}(I\boldsymbol{\omega} + AJ\boldsymbol{\Omega}) \tag{5}$$

where $\boldsymbol{M}^{\text{cm}}$ is the external moment relative to the spacecraft center of mass and the matrix $\omega^{\times}$ is the cross product matrix, which is given by

$$\omega^{\times} \equiv \begin{bmatrix} 0 & -\omega_z & \omega_y \\ \omega_z & 0 & -\omega_x \\ -\omega_y & \omega_x & 0 \end{bmatrix} \tag{6}$$

Application of Euler's law to the reaction wheels (with components in the reaction wheel frames) results in

$$JA^{-1}\dot{\boldsymbol{\omega}} + J\dot{\boldsymbol{\Omega}} = \boldsymbol{u} - f\boldsymbol{\Omega} \tag{7}$$

Now we decouple Eqs. (5) and (7) to recover the desired EOMs:

$$\tilde{I}\dot{\boldsymbol{\omega}} = \boldsymbol{M}^{\mathrm{cm}} - \omega^{\times} I\boldsymbol{\omega} - \omega^{\times} AJ\boldsymbol{\Omega} - A\boldsymbol{u} + Af\boldsymbol{\Omega} \tag{8}$$

$$\tilde{I}A\dot{\boldsymbol{\Omega}} = IAJ^{-1}\boldsymbol{u} - IAJ^{-1}f\Omega + \omega^{\times} I\omega + \omega^{\times} AJ\Omega - \boldsymbol{M}^{\mathrm{cm}} \tag{9}$$

where

$$\tilde{I} \equiv I - AJA^{-1} \tag{10}$$

In this study, the external moment $\boldsymbol{M}^{\mathrm{cm}}$ is simply the atmospheric torque. For the MGS model,[5] the $+X$ axis has a moment proportional to β, and the $+Y$ axis has a moment proportional to α. Thus, the atmospheric torque term is

$$\boldsymbol{M}^{\mathrm{cm}} = \tfrac{1}{2}\rho V_{\mathrm{rel}}^{2} SL \begin{bmatrix} C_{M_X}(\beta) & C_{M_Y}(\alpha) & 0 \end{bmatrix}^{T} \tag{11}$$

Inertial EOMs

The spacecraft's inertial attitude is determined from the quaternion kinematic equation

$$\dot{\boldsymbol{q}} = \tfrac{1}{2}\omega_{Q}\boldsymbol{q} \tag{12}$$

where

$$\omega_Q = \begin{bmatrix} 0 & \omega_z & -\omega_y & \omega_x \\ -\omega_z & 0 & \omega_x & \omega_y \\ \omega_y & -\omega_x & 0 & \omega_z \\ -\omega_x & -\omega_y & -\omega_z & 0 \end{bmatrix} \tag{13}$$

Relative EOMs

Because the momentum EOMs are a function of the aerodynamic angles α and β [from Eqs. (8) and (11)], we need to derive EOMs for these angles to analyze the behavior of the system conveniently. The EOMs we derive are not actually integrated in the simulation because the inertial attitude and position are sufficient to calculate the α and β. The motivation for this analysis is to linearize the relative attitude EOMs for use in our linear feedback controller.

We note that the relative wind angles α and β can be thought of as two Euler angles. These angles are measured relative to the relative wind vector. When $\alpha = \beta = 0$, the spacecraft points directly into the wind. The third Euler angle needed to complete the sequence is roll (ψ, about the $+Z$ spacecraft axis), which must be the first rotation in the sequence. By choosing the second and third rotations as angle of attack α and sideslip β, respectively, we find that the aerodynamic properties of α and β are preserved. This 321 Euler sequence is oriented with respect to the relative wind, that is, the velocity vector, which is not inertially fixed. Thus, we must include another rotation, χ, to transform inertial unit vectors into relative wind vectors. The inertial velocity vector orientation in the orbit plane is given by the angle $\chi \equiv \theta - \gamma$.

The inertial frame directions are chosen to match the spacecraft attitude when $\alpha = \beta = \psi = 0$. Thus, $\hat{x}_1$ points to the ascending node of the orbit, $\hat{y}_1$ points away from the orbital momentum vector, and $\hat{z}_1$ completes a right-handed sequence by pointing to a location in the orbital plane 90 deg ahead of the ascending node. With this definition $\dot{\boldsymbol{\chi}} = -\dot{\chi}\hat{y}_1$.

The direction cosine matrix mapping from inertial coordinates to body-fixed coordinates is

$$D = D_{\beta} D_{\alpha} D_{\psi} D_{\chi} \tag{14}$$

where

$$D_{\chi} = \begin{bmatrix} \cos\chi & 0 & \sin\chi \\ 0 & 1 & 0 \\ -\sin\chi & 0 & \cos\chi \end{bmatrix} \tag{15}$$

$$D_{\psi} = \begin{bmatrix} \cos\psi & \sin\psi & 0 \\ -\sin\psi & \cos\psi & 0 \\ 0 & 0 & 1 \end{bmatrix} \tag{16}$$

$$D_{\alpha} = \begin{bmatrix} \cos\alpha & 0 & -\sin\alpha \\ 0 & 1 & 0 \\ \sin\alpha & 0 & \cos\alpha \end{bmatrix} \tag{17}$$

$$D_{\beta} = \begin{bmatrix} 1 & 0 & 0 \\ 0 & \cos\beta & \sin\beta \\ 0 & -\sin\beta & \cos\beta \end{bmatrix} \tag{18}$$

The expression for the angular rates is given by

$$\boldsymbol{\omega} = \dot{\boldsymbol{\beta}} + \dot{\boldsymbol{\alpha}} + \dot{\boldsymbol{\psi}} + \dot{\boldsymbol{\chi}} \tag{19}$$

$$\boldsymbol{\omega} = \begin{bmatrix} \dot\beta \\ 0 \\ 0 \end{bmatrix} + D_{\beta}\begin{bmatrix} 0 \\ \dot\alpha \\ 0 \end{bmatrix} + D_{\beta}D_{\alpha}\begin{bmatrix} 0 \\ 0 \\ \dot\psi \end{bmatrix} - D_{\beta}D_{\alpha}D_{\psi}\begin{bmatrix} 0 \\ \dot\chi \\ 0 \end{bmatrix} \tag{20}$$

$$\begin{bmatrix} \omega_x \\ \omega_y \\ \omega_z \end{bmatrix} = \begin{bmatrix} 1 & 0 & -s_{\alpha} \\ 0 & c_{\beta} & c_{\alpha}s_{\beta} \\ 0 & -s_{\beta} & c_{\alpha}c_{\beta} \end{bmatrix}\begin{bmatrix} \dot\beta \\ \dot\alpha \\ \dot\psi \end{bmatrix} - \begin{bmatrix} c_{\alpha}s_{\psi} \\ s_{\alpha}s_{\beta}s_{\psi} + c_{\beta}c_{\psi} \\ s_{\alpha}c_{\beta}s_{\psi} - s_{\beta}c_{\psi} \end{bmatrix}\dot\chi \tag{21}$$

where $s_{\alpha} \equiv \sin\alpha$, $c_{\alpha} \equiv \cos\alpha$, etc.

This system is then solved for the Euler angular rates to yield the relative attitude EOMs in Eq. (22):

$$\begin{bmatrix} \dot\beta \\ \dot\alpha \\ \dot\psi \end{bmatrix} = \begin{bmatrix} 1 & s_{\beta}\tan\alpha & c_{\beta}\tan\alpha \\ 0 & c_{\beta} & -s_{\beta} \\ 0 & s_{\beta}/c_{\alpha} & c_{\beta}/c_{\alpha} \end{bmatrix}\left\{\begin{bmatrix} \omega_x \\ \omega_y \\ \omega_z \end{bmatrix} + \dot\chi\begin{bmatrix} c_{\alpha}s_{\psi} \\ s_{\alpha}s_{\beta}s_{\psi} + c_{\beta}c_{\psi} \\ s_{\alpha}c_{\beta}s_{\psi} - s_{\beta}c_{\psi} \end{bmatrix}\right\} \tag{22}$$

From Vinh et al.,[16] we deduce that

$$\dot\chi = \mu\cos\gamma / r^{2}V \tag{23}$$

We can compute the relative wind angles by performing the inverse operation of Eq. (14). The direction cosine matrix D is obtained from the inertial attitude quaternion $\boldsymbol{q}$ using the standard transformation:

$$D_{\mathrm{rel}} = DD_{\chi}^{-1} \tag{24}$$

$$D_{\mathrm{rel}} = \begin{bmatrix} c_{\alpha}c_{\psi} & c_{\alpha}s_{\psi} & -s_{\alpha} \\ s_{\alpha}s_{\beta}c_{\psi} - c_{\beta}s_{\psi} & s_{\alpha}s_{\beta}s_{\psi} + c_{\beta}c_{\psi} & c_{\alpha}s_{\beta} \\ s_{\alpha}c_{\beta}c_{\psi} + s_{\beta}s_{\psi} & s_{\alpha}c_{\beta}s_{\psi} - s_{\beta}c_{\psi} & c_{\alpha}c_{\beta} \end{bmatrix} \tag{25}$$

Thus, the Euler wind angles are given by

$$\tan\psi = \frac{d_{\mathrm{rel}}[1,2]}{d_{\mathrm{rel}}[1,1]} \tag{26}$$

$$\tan\alpha = \frac{-d_{\mathrm{rel}}[1,3]}{\sqrt{d_{\mathrm{rel}}^{2}[1,1] + d_{\mathrm{rel}}^{2}[1,2]}} \tag{27}$$

$$\tan\beta = \frac{d_{\mathrm{rel}}[2,3]}{d_{\mathrm{rel}}[3,3]} \tag{28}$$

The natural motion of the relative wind angles can be examined by setting $\boldsymbol{\omega}$ to $\boldsymbol{0}$ and setting the sideslip angle β and roll angle ψ to 0 as well. Equations (22) and (23) collapse to

$$\dot\beta = \dot\psi = 0 \tag{29}$$

$$\dot\alpha = \dot\chi \tag{30}$$

We note from Eq. (23) that $\dot\chi > 0$ during the drag pass. Thus, the angle of attack will naturally increase as the spacecraft orbits the planet. This increase is because the spacecraft attitude tends to remain fixed with respect to an inertial reference frame. The exact solution to the attitude EOMs will have an oscillating component, but without any control along the pitch axis, the angle of attack would be biased in the positive direction. From Eq. (11), we conclude that, with an uncontrolled attitude, momentum will tend to accumulate along the pitch axis during each drag pass. An attitude control is necessary to prevent the buildup of momentum.

Reaction Wheel Control Laws

The reaction wheel control laws can be divided into two types: exoatmospheric and atmospheric. In exoatmospheric flight, the reaction wheels are commanded to maintain an inertial attitude. For atmospheric flight, we investigate three control laws: spin down, affine partial state, and two stage.

Inertial Attitude Hold Controller

In normal spacecraft operation, the spacecraft is held in an inertially fixed attitude to either conduct science experiments or communicate with Earth. In our scheme, the spacecraft prepares for a drag pass by slewing into a new inertially fixed attitude such that the spacecraft is pointing into the relative wind on entry. As the spacecraft descends toward periapsis, the angle of attack increases, and the total system angular momentum changes as it is subjected to a growing aerodynamic torque. Because the reaction wheels are commanded to maintain an inertial attitude, the change in momentum is transferred to the reaction wheels. Thus, the spacecraft senses atmospheric entry when the commanded torque magnitude exceeds some threshold. (In our simulations, we use a threshold of 5% maximum torque.) After this threshold is exceeded, the reaction wheel switches to an atmospheric control mode. (Here we note again that the only instrumentation assumed are gyros to measure the angular velocities. It seems clear, however, that an accelerometer would significantly aid in the detection of atmospheric entry.)

Once atmospheric entry is detected, an onboard timer is started. This timer's purpose is to countdown the time until the spacecraft should reach periapsis (which is needed for some control laws) and also to countdown the time until the spacecraft should exit the atmosphere. On atmospheric exit, the reaction wheels once again switches modes, this time, back to the inertial attitude hold mode.

Spin-Down Controller

This control law despins the yaw and pitch reaction wheels during the atmospheric flythrough. When zero-spin rate is reached, the applied reaction wheel torques are shut off. After exiting the atmosphere, all residual spacecraft momentum is transferred back to the reaction wheels.

This mechanism works because the spacecraft can torque against the atmosphere. The atmosphere tends to keep the spacecraft in place (the angle of attack and sideslip angles oscillating about zero) while the wheels are desaturated. This control law works best if started near periapsis, where the atmosphere is densest. Before the spacecraft reaches its estimated periapsis, the commanded torque is zero, thus allowing the spacecraft to weathervane (undamped) back and forth into the relative wind. Shortly before periapsis, the pitch and yaw axis reaction wheels are despun at maximum available torque. Afterward, the commanded torque is again set to zero until exit. To ensure the reaction wheels have enough time to despin, each reaction wheel begins its momentum dump such that the dump will be half completed during the estimated periapsis passage.

Because the roll axis has no opposing external moment to torque against, any change in momentum along that axis will not be altered by the atmosphere. Any momentum storage along the roll axis will either have to be removed propulsively, or by creating an external moment by rotating the solar panels.

This control law has the advantage of being simple to implement and being independent of spacecraft and planetary parameters. It is also one of the best performing control laws for the six-degree-of-freedom case.

Affine Partial-State Controller

For this approach, we devise a linear state-feedback controller to drive the total system momentum to zero. We first need to linearize the attitude EOMs and pick a feedback gain matrix K to produce a stable closed-loop system, using only the measurable states ($\boldsymbol{\omega}$, $\boldsymbol{\Omega}$) as feedback. The derivation of this controller is presented in the next section.

Linearization of Equations of Motion

The angular momentum from Eq. (4) is a linear combination of the spacecraft and reaction wheel angular rates. The EOMs for the spacecraft angular rates [Eq. (8)] is a function of the Euler wind angles. Thus, we need to linearize Eqs. (8–10).

The first step in linearization is to choose the desired equilibrium conditions and to redefine the state variables as appropriate. One such set of equilibrium conditions is

$$\alpha^e = \beta^e = \psi^e = 0 \tag{31}$$

$$\boldsymbol{\omega}^e = [0 \quad -\dot{\chi} \quad 0]^T \tag{32}$$

$$\boldsymbol{\Omega}^e = J^{-1}A^{-1}I[0 \quad \dot{\chi} \quad 0]^T \tag{33}$$

$$\boldsymbol{u}^e = f\boldsymbol{\Omega}^e \tag{34}$$

Let $\boldsymbol{E}$ be the column vector of Euler angles

$$\boldsymbol{E} = [\beta \quad \alpha \quad \psi]^T \tag{35}$$

The state variables are then redefined by subtracting out their equilibrium values. Let $\boldsymbol{x}$ be the column vector of state variables, and $\delta\boldsymbol{x} \equiv \boldsymbol{x} - \boldsymbol{x}^e$, where $\boldsymbol{x} \equiv [\boldsymbol{E}, \boldsymbol{\omega}, \boldsymbol{\Omega}]^T$.

The linearized system of equations can be written as

$$\delta\dot{\boldsymbol{x}} = A(\rho)\delta\boldsymbol{x} + B\delta\boldsymbol{u} \tag{36}$$

$$\boldsymbol{H} = C\delta\boldsymbol{x} \tag{37}$$

Alternatively, we can write the system in affine form using the original state variables as

$$\dot{\boldsymbol{x}} = A(\rho)\boldsymbol{x} + B\boldsymbol{u} + F \tag{38}$$

$$\boldsymbol{H} = C\boldsymbol{x} \tag{39}$$

where

$$A = \begin{bmatrix} -\omega^{\times^e} & 1 & 0 \\ \tilde{I}^{-1}\dfrac{\partial \boldsymbol{M}}{\partial \boldsymbol{E}} & -\tilde{I}^{-1}\omega^{\times^e} I & \tilde{I}^{-1}(Af - \omega^{\times^e} AJ) \\ -A^{-1}\tilde{I}^{-1}\dfrac{\partial \boldsymbol{M}}{\partial \boldsymbol{E}} & A^{-1}\tilde{I}^{-1}\omega^{\times^e} I & A^{-1}\tilde{I}^{-1}(\omega^{\times^e} AJ - IAJ^{-1}f) \end{bmatrix} \tag{40}$$

$$B = [\mathbf{0} \quad -\tilde{I}^{-1}A \quad A^{-1}\tilde{I}^{-1}IAJ^{-1}]^T \tag{41}$$

$$C = [0 \quad I \quad AJ] \tag{42}$$

$$F = [-\boldsymbol{\omega}^e \quad \mathbf{0} \quad \mathbf{0}]^T \tag{43}$$

The control law is in the form of $\delta\boldsymbol{u} = K\delta\boldsymbol{x}$, or in terms of original state/control variables,

$$\boldsymbol{u} = K\boldsymbol{x} - K\boldsymbol{x}^e + \boldsymbol{u}^e \tag{44}$$

where K is the feedback control gain of the form

$$K = [K_{\boldsymbol{E}} \quad K_{\boldsymbol{\omega}} \quad K_{\boldsymbol{\Omega}}] \tag{45}$$

We have 9 states, 3 controls, and, thus, 27 feedback gains to choose. Because we cannot measure the (noninertial) Euler angles, we set the nine parameters from K_E to zero. We need a method to select the remaining 18 feedback gains to stabilize the closed-loop system. Because momentum cannot be removed from the roll axis, we set those coefficients to zero. Also, because the pitch and yaw axes are uncoupled in the linearized model, we set the cross terms to zero as well. This leaves us with four gains to choose (two for the pitch axis and two for the yaw axis).

Because our A matrix is time varying, negative instantaneous eigenvalues are insufficient for stability. To achieve stability in the nonlinear time-varying system, we take a minimax approach, where we pick the gain matrix such that the maximum real part of the closed-loop eigenvalues is a minimum. We note that the equilibrium conditions in Eqs. (32) and (33) are functions of $\dot{\chi}$, which is itself a function of the orbit. Of course, the orbital parameters will change during the aerobraking process. To avoid onboard updates of the parameter $\dot{\chi}$ after every drag pass, we tune the equilibrium point to the particular orbit corresponding to an eccentricity of 0.4. We find this approach to be robust even considering the large changes in eccentricity throughout aerobraking. Alternatively, the equilibrium point could be retuned each orbit, but results indicate that a statically tuned equilibrium point works sufficiently well.

For the special case where the reaction wheels are aligned with the spacecraft principal axes (which are identical to the yaw, pitch, and roll axes), the minimax problem has the analytic solution

$$K_{\omega,x} = \left(3\tilde{I}_x - \frac{1}{3}I_x\right)\sqrt{\frac{-q_p SLC_{M_X}}{3\tilde{I}_x}} \tag{46}$$

$$K_{\omega,y} = \left(3\tilde{I}_y - \frac{1}{3}I_y\right)\sqrt{\frac{-q_p SLC_{M_Y}}{3\tilde{I}_y}} \tag{47}$$

$$K_{\Omega,x} = f - \frac{J_y}{3}\sqrt{\frac{-q_p SLC_{M_X}}{3\tilde{I}_x}} \tag{48}$$

$$K_{\Omega,y} = f - \frac{J_y}{3}\sqrt{\frac{-q_p SLC_{M_Y}}{3\tilde{I}_y}} \tag{49}$$

Theorem

In the aforementioned special case, the body-fixed axes are decoupled in the linearized system and can be treated individually. For both of the controllable axes, the affine partial-state controller uses feedback from the two measurable state variables, ω and Ω. Without being able to measure the third state variable α, the closed-loop system poles cannot be arbitrarily placed. For any monic polynomial with exactly one specified coefficient, the minimax solution occurs when the roots are real and identical.

Proof by Contradiction

Consider the monic polynomial ($c_n = 1$) given by

$$p(s) = \sum_{k=0}^{n}\binom{n}{k}c_k^{n-k}s^k \tag{50}$$

If the jth term is the only specified term, then the minimax solution is given by $c_k = c_j$ for all k, which yields

$$p_j(s) = \sum_{k=0}^{n}\binom{n}{k}c_j^{n-k}s^k \tag{51}$$

so that

$$p_j(s) = (s + c_j)^n \tag{52}$$

Let us assume that $p_j(s)$ is not the minimax solution; in other words, every root of $p(s)$ has a real part smaller than c_j. We will call this better polynomial $q(s)$,

$$q(s) = \sum_{k=0}^{n}\binom{n}{k}d_k^{n-k}s^k \tag{53}$$

or

$$q(s) = \prod_{i=1}^{n}(s + c_j + \epsilon_i) \tag{54}$$

Our constraints are that $d_j = c_j$ (fixed jth term) and $\Re\{\epsilon_i\} > 0$ for all i. [We need every root of $q(s)$ to be smaller than c_j.] Expansion of Eq. (54) reveals that

$$\binom{n}{j}d_j^{n-j} = \sum_{k=1}^{\binom{n}{j}}\prod_{i=1}^{n-j}(c_j + \epsilon_{k_i}) \tag{55}$$

but

$$\binom{n}{j}d_j^{n-j} > \binom{n}{j}c_j^{n-j} \tag{56}$$

so that

$$d_j > c_j \tag{57}$$

However, our original assumption was that $d_j = c_j$, that is, the jth term was fixed, and so we have a contradiction. Therefore, if a polynomial has exactly one coefficient that is fixed, with the rest arbitrary, then the polynomial that minimizes the maximum real part of the roots is the polynomial with n repeated real roots.

Application to the Affine Partial-State Controller

The characteristic polynomial (for the pitch axis) for the closed-loop system is

$$s^3 + s^2\left(\frac{I_y f}{\tilde{I}_y J_y} - \frac{I_y K_\Omega}{\tilde{I}_y J_y} + \frac{K_\omega}{\tilde{I}_y}\right) - s\left(\frac{q_p SLC_{M_Y}}{\tilde{I}_y}\right) + \left(\frac{q_p SLC_{M,Y}}{\tilde{I}_y}\right)\left(\frac{K_\Omega - f}{J_y}\right) = 0 \tag{58}$$

(We note that the yaw-axis characteristic polynomial is identical but with X-axis parameters instead of the Y-axis ones.)

In Eq. (58), the s coefficient is fixed (no feedback available). Because the s term is the only such term, we know the minimax solution occurs when all roots are real and identical. From Eq. (58), we deduce the (triple-root) closed-loop eigenvalue to be

$$s = -\sqrt{\frac{-q_p SLC_{M_Y}}{3\tilde{I}_y}} \tag{59}$$

The required feedback coefficients are, thus, given by Eqs. (46–49).

Two-Stage Controller

The affine partial-state controller performs nearly all of its work by the time the spacecraft reaches periapsis. In thick atmospheres, the controller quickly drives the system to the equilibrium condition. In thin atmospheres, the affine partial-state controller is too sluggish to fully desaturate the reaction wheels. However, the spin-down controller can rapidly despin the wheels. Furthermore, the spin-down controller performs best when activated near periapsis. The advantages of these two controllers inspire us to define a two-stage control law, which is a combination of the two laws. The first stage uses the affine partial-state control law and is activated on atmospheric entry. The second stage uses the spin-down logic and is activated at estimated periapsis.

In the cases where the first stage is able to remove completely the system momentum, the spacecraft and reaction wheels have a nonzero equilibrium angular rate [Eqs. (32) and (33)]. We modify the spin-down stage to spin down to the affine partial-state equilibrium point. Thus, in the nominal cases, the two-stage controller performs as well as the affine partial-state controller.

Table 2 Reference simulation parameters

Parameter	Reference value
Eccentricity	0.4
Dynamic pressure at periapsis	0.5 N/m^2
Stored momentum[a]	13.5 $kg \cdot m^2/s$
Atmospheric density	100% nominal
Entry angle of attack	0 deg
Entry sideslip angle	0 deg

[a]Along pitch ($+Y$) axis at 50% capacity.

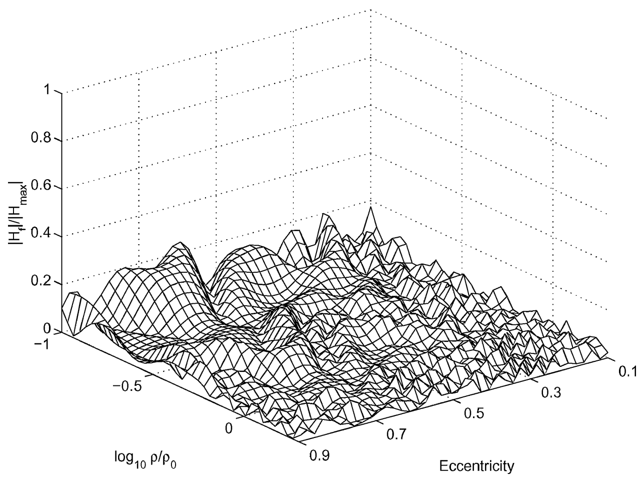

Fig. 3 Fractional momentum remaining after a drag pass for the spin-down controller where the indepedent variables are relative density and eccentricity.

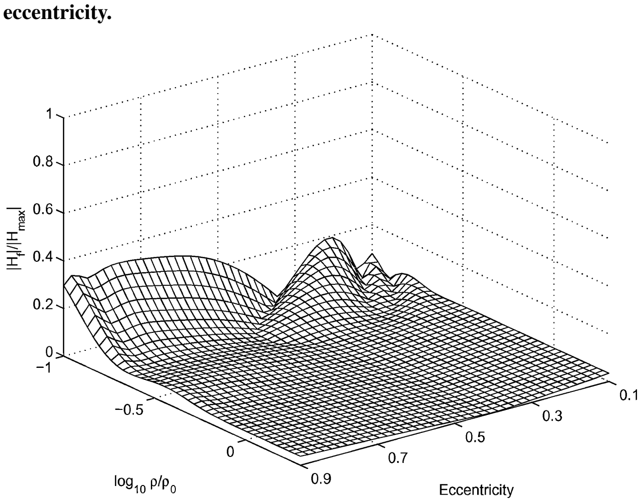

Fig. 4 Fractional momentum remaining using the affine partial-state controller.

Results

Overview

We judge the effectiveness of a particular control law by the angular momentum reduction achieved during the drag pass. There are several parameters that influence the performance of our control laws. As we consider the variations in the most influential parameters, we find it convenient to establish a set of reference parameters listed in Table 2.

Single Pass

The most important parameters that affect our control laws are the atmospheric density and the orbit eccentricity. Figures 3–5 illustrate the performance of the three control laws. The height of the mesh represents the fractional momentum remaining after a drag pass, where the initial stored momentum is at 50% capacity. The spin-down case (Fig. 3) usually removes about 90% of the stored momentum. It is somewhat less effective in a thin atmosphere. In this case, the spacecraft does not sense atmospheric entry until relatively late in the drag pass. As a result, the periapsis timer is started late, and the spin-down controller barely has enough time to complete its momentum dump. However, if the controller is started too early in the nominal or thick atmosphere cases, there will not be enough external torque to oppose the spacecraft's angular momentum. This condition will result in high-amplitude oscillations about the pitch and yaw axes, which will cause the spacecraft to gain momentum instead of to lose it.

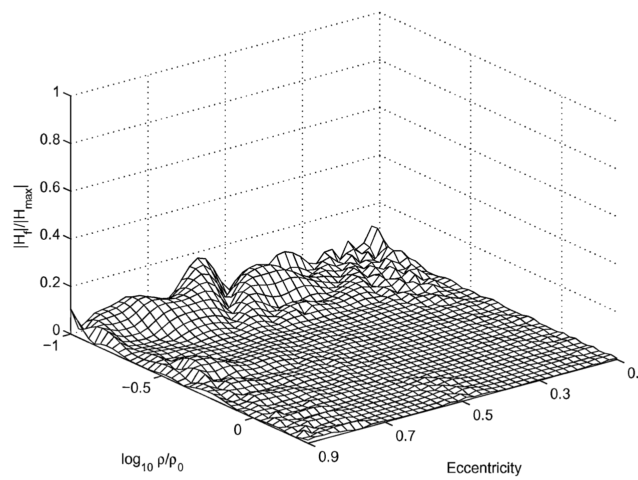

Fig. 5 Fractional momentum remaining using the two-stage controller.

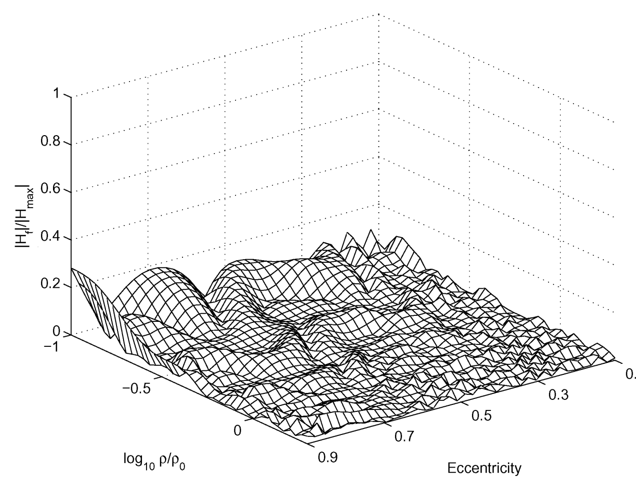

Fig. 6 Fractional momentum remaining using the spin-down controller where initial stored momentum is along the pitch (+*Y*) axis at 27 $kg \cdot m^2/s$ (100% capacity).

The affine partial-state control law (Fig. 4) is able to remove nearly 100% of the total momentum in most cases. It has trouble in the low-density case but still works better than the spin down. In the worst case ($\log_{10} \rho/\rho_0 = -1$, $e = 0.9$), spin down removes only 20% of the stored momentum, whereas the affine partial state removes about 65% of the momentum. The tuning of the affine partial state about an eccentricity of 0.4 is also evident in Fig. 4 as a slight upward slope in the mesh surface away from the line $e = 0.4$.

Finally, the two-stage control law (Fig. 5) demonstrates the best of both preceding controllers. The mesh is flat like the affine partial state, but without the slope. In the worst case, the controller removes over 80% of the stored momentum.

We present an extreme case in Figs. 6–8. Figures 6–8 show the fractional momentum remaining for the three control laws when the initial momentum wheel (along the pitch axis) is 100% saturated. All three control laws are able to reduce substantially the momentum for every eccentricity and atmospheric density considered.

All three control laws perform well under a variety of atmospheric uncertainties. Table 3 summarizes the average and worst-case performance of the three laws. The spin-down and affine partial-state

Table 3 Performance summary of control laws in terms of initial and final saturation

		Final saturation, %		
Initial, %	Statistic	Spin down	Affine	Two stage
0	Mean	0.9	1.1	0.3
	Maximum	3.1	2.6	1.4
25	Mean	2.9	2.0	1.1
	Maximum	11.1	12.1	6.8
50	Mean	2.5	2.0	0.8
	Maximum	12.2	16.4	8.8
75	Mean	2.6	1.8	1.3
	Maximum	12.6	7.9	9.0
100	Mean	3.6	3.2	2.0
	Maximum	28.2	26.5	15.6

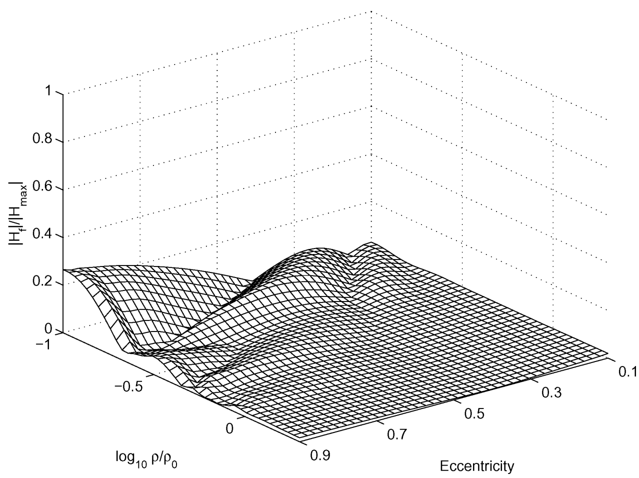

Fig. 7 Fractional momentum remaining using the affine partial-state controller.

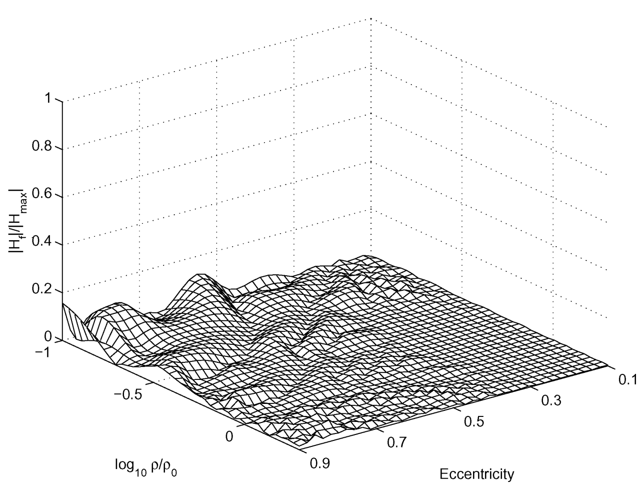

Fig. 8 Fractional momentum remaining using the two-stage controller.

controllers have similar performance for low saturations, whereas the affine partial state is usually better for higher initial saturations. The two-stage controller is uniformly the best control law in almost all test cases, making it the most robust control law of the three.

We note that other spacecraft parameters, for example, the reference length, area, moment coefficient, moment of inertia, are dynamically equivalent to the atmospheric density.[17] Thus, the control law behavior with spacecraft parameter uncertainties is identical to the behavior with a proportionately scaled atmospheric density.

Multiple Passes

A controller may work well over a single drag pass but fail over the duration of the entire aerobraking phase. Thus, we simulate an entire aerobraking mission using each of the controllers. The spacecraft is assumed to capture into an initial 48-h orbit and then to aerobrake into a 2-h final orbit. Outside the atmosphere, space environmental torques are applied to the spacecraft (at a rate of 5×10^{-6} N · m) along all three axes.

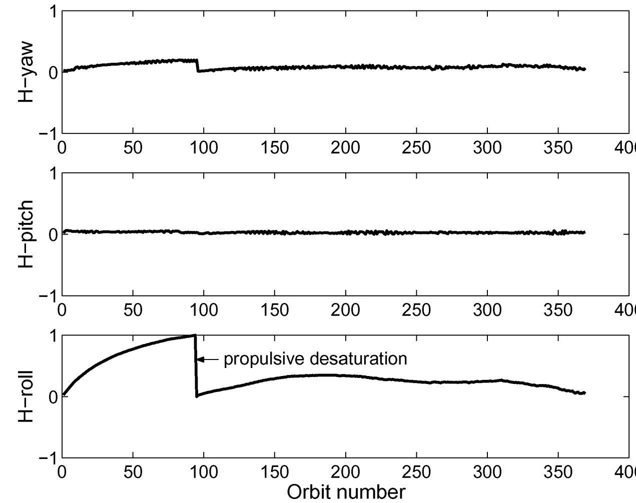

Fig. 9 Momentum of the spacecraft after each drag pass using the spin-down controller with an initial orbit period of 48 h and a final orbit period of 2 h.

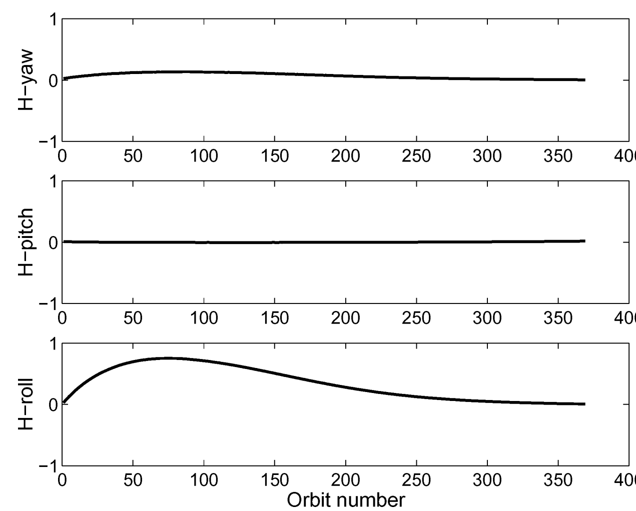

Fig. 10 Momentum of the spacecraft after each drag pass using the affine partial-state controller.

Figures 9–11 illustrate the stored angular momentum along each axis after each atmospheric-flythrough orbit. From the linearized EOM (38–40), we see that the yaw, X, and roll, Z, axes are coupled. Even though the roll axis is not directly controlled, any control inputs or disturbances that affects one of these axes will also affect the other. Furthermore, after each drag pass, the spacecraft must slew to a new inertial attitude. The pitch axis will tend to remain inertially fixed from orbit to orbit (because the orbital angular momentum vector tends to remain inertially fixed). Thus, the net effect of the spacecraft's reorientation is that a component of the stored momentum is swapped between the yaw and roll axes. The effect becomes more pronounced as the orbit decays (and thus, the atmospheric turn angle increases). This result is beneficial (and fortuitous) because the roll-axis momentum can be passively controlled through the yaw axis.

In Fig. 9, we observe that the disturbance torques on the roll axis accumulate beyond the reaction wheel's capacity to store it. Thus, a propulsive desaturation of the roll-axis reaction wheel (RW) is required.

The affine partial-state controller (Fig. 10) and the two-stage controller (Fig. 11) are able to control the yaw-axis momentum much

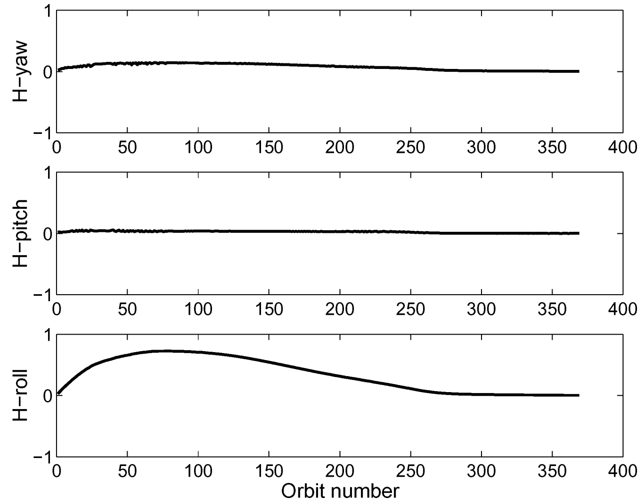

Fig. 11 Momentum of the spacecraft after each drag pass using the two-stage controller.

better than the spin-down controller. As expected, the roll axis does not suffer as much. During the slewing maneuver after a drag pass, the yaw axis does not have any appreciable component to be mapped into the roll axis, and the roll axis is able to lose some momentum by its component that is mapped to the yaw axis.

Roll Axis

Even with passive roll-momentum management, the roll-axis reaction wheel may easily saturate if the space environmental torques are sufficiently large. We would, therefore, like to manage more actively the roll-axis momentum during each drag pass.

If the solar panels are attached at an angle relative to the Y–Z plane, the relative wind can induce a propeller torque on the body $+Z$ axis (the roll axis). Because the torque on the roll axis will always be in same direction, the angular momentum buildup will be secular.

The current practice is to use propellant to manage the spacecraft's momentum. With our two-axis control laws, propellant would only be needed to manage the roll-axis momentum. Another scheme to manage the roll-axis momentum is to articulate the solar panels to control the rolling moment. This controller would control the pitch angle of the propellor blades (solar panels) to first annihilate the roll-axis momentum and then null out the rolling moment.

Conclusions

All three of the considered control laws are capable of managing the spacecraft angular momentum. The spin-down case is conceptually the simplest of these three control laws and has the advantage of being independent of spacecraft properties. However, the spin-down controller does require timing information on periapsis, which is particularly critical for high-eccentricity orbits and high initial stored momentum. The affine partial-state controller is the easiest to implement, needing only five constant parameters to describe it fully. These parameters are functions of spacecraft inertia, aerodynamic moment coefficients, and projected atmospheric density. Because this controller does not require any timing information, it is the least memory-intensive controller of the three. Finally, the two-stage controller provides performance superior to its two component laws, but at the combined complexity of the two.

Acknowledgments

This work was funded in part by the Purdue Research Foundation and the Jet Propulsion Laboratory (JPL), California Institute of Technology, Pasadena, California, under JPL Contract 1223406 (G. T. Rosalia, Contract Manager, and Dennis V. Byrnes, Technical Manager). Portions of the work described were performed at JPL California Institute of Technology, under contract with NASA.

References

[1]Munk, M., and Powell, R., "Aeroassist Technology Planning for Exploration," *Advances in the Astronautical Sciences*, Vol. 105, Pt. 2, 2000, pp. 1073–1083.

[2]Spencer, D., and Braun, R., "Mars Pathfinder Atmospheric Entry: Trajectory Design and Dispersion Analysis," *Journal of Spacecraft and Rockets*, Vol. 33, No. 5, 1996, pp. 670–676.

[3]Lyons, D., "Aerobraking at Venus and Mars, a Comparison of the Magellan and Mars Global Surveyor Aerobraking Phases," *Advances in the Astronautical Sciences*, Vol. 103, Pt. 1, 1999, pp. 859–878.

[4]Lyons, D., Beerer, J., Esposito, P., Johnston, M., and Willcockson, W., "Mars Global Surveyor: Aerobraking Mission Overview," *Journal of Spacecraft and Rockets*, Vol. 36, No. 3, 1999, pp. 307–313.

[5]Wilmoth, R. G., Rault, D. F., Cheatwood, F. M., Engelund, W. C., and Shane, R. W., "Rarefied Aerothermodynamic Predictions for Mars Global Surveyor," *Journal of Spacecraft and Rockets*, Vol. 36, No. 3, 1999, pp. 314–322.

[6]Lyons, D., "Aerobraking Magellan: Plan Versus Reality," *Advances in the Astronautical Sciences*, Vol. 87, No. 2, 1994, pp. 663–680, also AAS Paper 94-118, Feb. 1994.

[7]Tragesser, S., and Longuski, J., "Analysis and Design of Aerocapture Tether with Accounting for Stochastic Errors," *Journal of Spacecraft and Rockets*, Vol. 35, No. 5, 1998, pp. 683–689.

[8]Tragesser, S., "Analysis and Design of Aerobraking Tethers," Ph.D. Dissertation, School of Aeronautics and Astronautics, Purdue Univ., West Lafayette, IN, Dec. 1997.

[9]Lyons, D., "Aerobraking Automation Options," *Advances in the Astronautical Sciences*, Vol. 109, Pt. 2, 2001, pp. 1231–1246.

[10]Johnson, W. R., Longuski, J. M., and Lyons, D. T., "Pitch Control During Autonomous Aerobraking for Near-Term Mars Exploration," *Journal of Spacecraft and Rockets*, Vol. 40, No. 3, 2003, pp. 371–379.

[11]Johnson, W., Longuski, J., and Lyons, D., "High-Fidelity Modeling of Semi-Autonomous Attitude Control During Aerobraking," American Astronautical Society, AIAA Paper 2002-4909, Aug. 2002.

[12]Bialke, B., "High Fidelity Mathematical Modeling of Reaction Wheel Performance," American Astronautical Society, AAS Paper 98-063, Feb. 1998.

[13]Justus, C., "Mars Global Reference Atmospheric Model for Mission Planning and Analysis," *Journal of Spacecraft and Rockets*, Vol. 28, No. 2, 1991, pp. 216–221.

[14]Justus, C., and Johnson, D., "Mars Global Reference Atmospheric Model 2001 Version (Mars-GRAM 2001): Users Guide," NASA TM-2001-210961, April 2001.

[15]Davies, M., Abalakin, V., Brahic, A., Bursa, M., Chovitz, B., Lieske, J., Seidelmann, P., Sinclair, A., and Tjuflin, Y., "Report of the IAU/IAG/COSPAR Working Group on Cartographic Coordinates and Rotational Elements of the Planets and Satellites: 1991," *Celestial Mechanics and Dynamical Astronomy*, Vol. 53, No. 4, 1992, pp. 377–397.

[16]Vinh, N., Busemann, A., and Culp, R., *Hypersonic and Planetary Entry Flight Mechanics*, Univ. of Michigan Press, Ann Arbor, MI, 1980, Chap. 3.

[17]Johnson, W. R., Longuski, J. M., and Lyons, D. T., "Nondimensional Analysis of Reaction-Wheel Control for Aerobraking," *Journal of Guidance, Control, and Dynamics*, Vol. 26, No. 6, 2003, pp. 861–868.

C. A. Kluever
Associate Editor